RSC Advances

PAPER

View Article Online
View Journal | View Issue

Cite this: *RSC Adv.*, 2015, **5**, 38774

Comparison of four different synthetic routes of $Ni_2P/TiO_2–Al_2O_3$ catalysts for hydrodesulfurization of dibenzothiophene†

Ruchao Wei, Qingqing Zhu, Fei Han, Qingxin Guan and Wei Li*

Received 30th January 2015
Accepted 8th April 2015

DOI: 10.1039/c5ra01899d

www.rsc.org/advances

$Ni_2P/TiO_2–Al_2O_3$ is a very promising hydrodesulfurization catalyst, however the catalysts reported so far all use the temperature-programmed reduction (H_2-TPR) method and the reduction temperature can be as high as 973 K. It is important to develop more feasible methods to prepare this material. Herein, $Ni_2P/TiO_2–Al_2O_3$ catalysts were successfully synthesized at a low reduction temperature (573 K) based on $NiCl_2·6H_2O$ and $NH_4H_2PO_2$ (method I). Three other methods were also used to prepare the $Ni–P/TiO_2–Al_2O_3$ catalysts in this work. The catalysts were characterized using XRD, TEM, FT-IR, XPS, CO uptake, and N_2 sorption measurements. Experimental results indicate that the preparation method had a major influence on the physicochemical properties of the catalysts and the HDS activity. Among the four methods examined, method I could more effectively suppress the formation of $AlPO_4$ and favor the formation of Ni_2P, which can be attributed to the relatively low reduction temperature and the flowing hydrogen used in this method. The hydrodesulfurization activity results indicate that the $Ni_2P/TiO_2–Al_2O_3$ catalyst prepared by method I gave a high HDS conversion of 100.0% at a reaction temperature of 583 K. The results suggest that method I provides a simple and energy-efficient route for the preparation of the $Ni_2P/TiO_2–Al_2O_3$ catalyst with excellent catalytic performance for the HDS of dibenzothiophene.

1. Introduction

Crude oil is becoming heavier, and this will worsen in the future; in addition, because of the growing demand for ultra clean fuels nowadays, it is an urgent issue to develop a more effective way to remove sulfur from oil fractions. Catalytic hydrodesulfurization (HDS) is an important technology for reducing the sulfur content in transportation fuels.[1,2] Transition metal phosphides have attracted considerable attention because of their excellent activity for the HDS of petroleum feedstocks. Among the metal phosphides studied, nickel phosphide (Ni_2P) has been shown to have the highest HDS activity.[3–5] However, the surface area of unsupported Ni_2P catalysts is rather low, and therefore the dispersion of Ni_2P on a high-surface support is needed.[3] Many supports, such as SiO_2,[3] Al_2O_3,[6] MCM-41,[7] and activated carbon,[8] have been reported as supports for Ni_2P catalysts.

In general, the supported Ni_2P catalyst is usually prepared from a nickel salt together with ammonium phosphate in hydrogen flow, which is known as the temperature-programmed reduction (H_2-TPR) method. The H_2-TPR method has proved to be a reliable way to prepare bulk and supported metal phosphides.[3,7–9] However, the H_2-TPR method requires strict temperature-programmed steps, long treatment time, and high temperatures (>873 K), which lead to large phosphide particles and low catalytic activity. In recent years, several other methods for synthesizing metal phosphides have been reported; these methods can be classified based on the phosphorus source used, such as the PH_3 method,[10] the triphenylphosphine method,[11–13] the hypophosphites method,[14–17] and the nickel dihydrogenphosphite method.[18–20] Moreover, supported Ni_2P has also been synthesized by the reduction of oxide precursors in hydrogen plasma.[21]

Macroporous γ-Al_2O_3 is widely used as a support for traditional oil HDS catalysts because of its relatively high surface area, good mechanical strength, high thermal stability, and low cost.[22–24] When γ-Al_2O_3 is used as a support for the Ni_2P catalyst, it is well known that phosphorus interacts strongly with γ-Al_2O_3, in many cases resulting in the formation of aluminum phosphates, such as $AlPO_4$, that can suppress the formation of the active sites, *i.e.*, the Ni_2P can cause serious damage to the activity of the supported Ni_2P catalysts.[25] To overcome this disadvantage, $TiO_2–Al_2O_3$ binary oxide has been proposed as a promising support for Ni_2P catalysts. Previous reports have demonstrated that the a $TiO_2–Al_2O_3$ composite support could weaken the interactions between phosphorus and γ-Al_2O_3, and

College of Chemistry, Key Laboratory of Advanced Energy Materials Chemistry (Ministry of Education), Collaborative Innovation Center of Chemical Science and Engineering (Tianjin), Nankai University, Tianjin, 300071, China. E-mail: weili@nankai.edu.cn; Fax: +86-22-23508662; Tel: +86-22-23508662

† Electronic supplementary information (ESI) available. See DOI: 101039/c5ra01899d

thus effectively prevent the formation of aluminum phosphates such as $AlPO_4$ at the surface of the support.[26–28]

As far as we know, the Ni_2P/TiO_2–Al_2O_3 catalysts reported so far all use the H_2-TPR method and the reduction temperature can be as high as 973 K. Because the Ni_2P/TiO_2–Al_2O_3 catalyst has great potential to be used as a highly effective HDS catalyst, it is important and useful to develop more feasible methods to prepare it. The aim of this work was to develop a more feasible way to prepare a highly active Ni_2P/TiO_2–Al_2O_3 catalyst for HDS of dibenzothiophene (DBT), and the main consideration is the synthetic temperature.

2. Experimental

2.1. Preparation of supports and catalysts

The γ-Al_2O_3 was obtained by the calcination of pseudoboehmite (Shandong Aluminum Plant, PR China) at 873 K for 2 h. The composite TiO_2–Al_2O_3 supports were prepared using the sol–gel method as described previously.[27] All of the TiO_2–Al_2O_3 supports used in this paper consisted of 30 wt% TiO_2. Hereafter, the support will be referred to as Ti/Al. The composite TiO_2–Al_2O_3-supported Ni–P catalysts were prepared using four different methods. All of the catalysts were prepared with a Ni_2P loading of 30 wt%.

The first method (method I) to prepare a Ni–P/TiO_2–Al_2O_3 catalyst involves two main steps: (1) the precursor is obtained by co-impregnation with an aqueous solution of an ammonium hypophosphite and nickel chloride solution with the composite TiO_2–Al_2O_3 supports, followed by drying; (2) the precursor is converted to nickel phosphide in flowing H_2.[17] In a typical experiment, the supported Ni–P/TiO_2–Al_2O_3 catalyst was obtained as follows. Initially, 13.73 g of $NiCl_2 \cdot 6H_2O$ and 7.20 g $NH_4H_2PO_2$ were dissolved in 80 mL of deionized water at room temperature to form a uniform solution (the initial molar ratio of P/Ni is 1.5). Then 10.0 g of the TiO_2–Al_2O_3 support was added to the solution and stirred for 8 h. The slurry was then evaporated at 65 °C and the precursor was obtained. The precursor was loaded into a quartz tube reactor and reduced by heating to the desired temperature at a rate of 10 K min^{-1} in a flow of H_2 (100 mL min^{-1}), held for 2 h, then naturally cooled to room temperature, followed by passivation for 2 h under flowing 1% O_2/N_2. Based on the initial P/Ni mole ratio and reduction temperature used, the catalysts were named Ni–P/Ti/Al–I-X-Y, where I, X, and Y represent the first method, the initial P/Ni mole ratio, and the reduction temperature, respectively.

In the second method (method II), a Ni–P/TiO_2–Al_2O_3 catalyst was synthesized by the decomposition of hypophosphite precursors using $NiCl_2 \cdot 6H_2O$ and $NaH_2PO_2 \cdot H_2O$ as the nickel source and phosphorus source, respectively. According to our previous work,[14] the same synthesis procedures and an optimal $H_2PO_2^-/Ni^{2+}$ mole ratio of 1.5 was employed. In a typical experiment, the supported Ni–P/TiO_2–Al_2O_3 catalyst was obtained as follows. Initially, 13.73 g of $NiCl_2 \cdot 6H_2O$ and 9.18 g $NaH_2PO_2 \cdot H_2O$ were dissolved in 80 mL of deionized water at room temperature to form a uniform solution (the initial molar ratio of P/Ni is 1.5, Ni_2P loading of 30 wt%). Then 10.0 g of the TiO_2–Al_2O_3 support was added to the solution and stirred for 8 h. The slurry was then evaporated at 353 K and the precursor was obtained. At the start, the air in the reactor was removed with flowing Ar, after which the resulting solid was heated to 573 K at a rate of 10 K min^{-1} and held at 573 K for 0.5 h in a static Ar atmosphere. The product was cooled to ambient temperature under Ar and was washed several times with deionized water to remove ion impurities, after which the wet material was dried at 393 K for 3 h. The catalyst was named Ni–P/Ti/Al–II, where II represents the second method used.

$(NH_4)_2HPO_4$ (or $NH_4H_2PO_4$) was used as the phosphorus source in the traditional H_2-TPR method to prepare a Ni_2P/TiO_2–Al_2O_3 catalyst and an initial Ni/P ratio of 1/2 was determined to be optimal for hydrodesulfurization as previously reported.[26,28] Recently, our group reported a simple and feasible method (DR method) for synthesizing bulk and supported nickel phosphides from oxide precursors.[29] The third method (method III) to prepare the supported Ni_2P catalysts was similar to our previous report and a PO_4^{3-}/Ni^{2+} mole ratio of 2.0 was employed. In a typical experiment, 16.80 g of $Ni(NO_3)_2 \cdot 6H_2O$ and 13.29 g of $NH_4H_2PO_4$ were dissolved in 60 mL of deionized water at room temperature to form a uniform solution (the initial molar ratio of P/Ni is 2.0, Ni_2P loading of 30 wt%). Then 10.0 g of the TiO_2–Al_2O_3 support was added to the solution and stirred for 8 h. The slurry was then evaporated at 393 K and calcined at 773 K for 2 h to obtain the precursor. Subsequently, the precursor and 10 mL of quartz sand were loaded into the quartz tube reactor (as a preliminary heating zone). The precursor materials were heated to 923 K at a rate of 10 K min^{-1} in flowing Ar. Then the gas was changed to flowing H_2 (60 mL min^{-1}) and the temperature was maintained at 923 K for 2 h. Finally, the product was cooled to ambient temperature under flowing H_2 and was passivated for 2 h under flowing 1% O_2/N_2. The catalyst was named Ni–P/Ti/Al–III, where III represents the third method.

For comparison, a fourth method, *i.e.*, the H_2-TPR method, was also used to prepare a Ni_2P/TiO_2–Al_2O_3 catalyst. In a typical experiment, 16.80 g of $Ni(NO_3)_2 \cdot 6H_2O$ and 13.29 g of $NH_4H_2PO_4$ were dissolved in 60 mL of deionized water at room temperature to form a uniform solution (the initial molar ratio of P/Ni is 2.0, Ni_2P loading of 30 wt%). Then 10.0 g of the TiO_2–Al_2O_3 support was added to the solution and stirred for 8 h. The slurry was then evaporated at 393 K and calcined at 773 K for 2 h to obtain the precursor. Subsequently, the precursor was loaded into the quartz tube reactor and the flow rate of H_2 was 150 mL min^{-1}. The temperature program was as follows: a heating rate of 5 K min^{-1} was used from room temperature to 673 K, then a heating rate of 1 K min^{-1} was used from 673 K to 923 K, and the temperature was maintained at 923 K for 2 h. Subsequently, the product was cooled to room temperature followed by passivation for 2 h under flowing 1% O_2/N_2. The catalyst was named Ni–P/Ti/Al–IV, where IV represents the fourth method.

2.2. Characterization methods

Powder X-ray diffraction (XRD) of the passivated sample was performed on a Bruker D8 focus diffractometer, with Cu Kα radiation at 40 kV and 40 mA. Powder diffractograms were

recorded at 12° min^{-1} scanning speed over a 2θ range of 10–80°. The BET surface area, pore volume, and pore size distribution of the samples were determined at liquid nitrogen temperature on a BEL-Mini adsorption analyzer. Before measuring, the passivated catalyst was degassed at 523 K for 3 h prior to the measurement. The adsorption isotherms for nitrogen were measured at 77 K. Transmission electron microscopy (TEM) images were acquired using a Philips Tecnai G^2 F-20 field emission gun transmission electron microscope. The passivated catalysts were dispersed in ethanol in an ultrasonic bath for several minutes. A drop of the catalyst suspension was placed on a copper grid coated with a carbon film, and left to dry before analysis. IR spectroscopy spectra were acquired with a Bruker Vector 22 instrument in the range of 400–4000 cm^{-1}. For skeletal spectra, pressed KBr disks were used. The solid specimens were generated *via* the conventional procedure, *i.e.* by pelletizing 2.0 mg of the catalyst with 200 mg of KBr. The X-ray photoelectron spectroscopy (XPS) spectra were acquired using a Kratos Axis Ultra DLD spectrometer employing a monochromated Al Kα X-ray source ($h\nu$ = 1486.6 eV), hybrid (magnetic/electrostatic) optics, and a multichannel plate and delay line detector. All of the XPS spectra were recorded using an aperture slot of 300 μm × 700 μm; survey spectra were recorded with a pass energy of 80 eV and high-resolution spectra with a pass energy of 40 eV. To subtract the surface charging effect, the C(1s) peak has been fixed at a binding energy of 284.6 eV. The CO uptake was measured using Micromeritics Chemisorb 2750 gas-adsorption equipment. Usually, 0.1 g of a passivated sample was loaded into a quartz reactor and pretreated in 10% H_2/Ar at 723 K for 3 h. After cooling in He, pulses of 10% CO/He in a He carrier (60 mL (NTP) min^{-1}) were injected at 303 K through a loop tube. CO pulses were repeatedly injected until no further CO uptake was observed after consecutive injections.

2.3. Catalytic activity test

The HDS catalytic activities were evaluated using 3000 ppm DBT in decalin. The HDS reaction was carried out in a high-pressure fixed-bed microreactor. The catalyst was pelleted, crushed, and sieved with 20–40 mesh. One gram of the catalyst was diluted with SiO_2 to a volume of 5.0 mL in the reactor. The testing conditions for the HDS reaction were 583 K, 3.0 MPa, weight hourly space velocity (WHSV) = 6 h^{-1}, and H_2/oil = 600/1 (v/v). Liquid products were collected every hour after a stabilization period of 8 h. Both feed and products were analyzed using gas chromatography (Agilent, 7890 A) equipped with a flame ionization detector and HP-5 column. The DBT conversion and turnover frequency (TOF) were used to evaluate the HDS activity. The TOF was calculated using eqn (1):[29]

$$\mathrm{TOF} = \frac{F_{\mathrm{Ao}}}{W}\frac{X_{\mathrm{A}}}{\mathrm{CO}_{\mathrm{uptake}}}, \quad (1)$$

where F_{Ao} is the molar rate of DBT fed into the reactor (μmol s^{-1}), W is the weight of the catalyst (g), X_{A} is the conversion of DBT (%), and $\mathrm{CO}_{\mathrm{uptake}}$ is the uptake of chemisorbed CO (μmol g^{-1}).

3. Results and discussion

3.1. X-ray diffraction analysis

XRD patterns of Ni–P/TiO_2–Al_2O_3 catalysts are shown in Fig. 1. All of the samples show a peak at 25.3° corresponding to the characteristic peak of anatase TiO_2 (PDF: 21-1272). For the samples prepared by method I, Ni–P/Ti/Al–I-1.5-573 K shows small peaks corresponding to Ni_2P. With an increase in the reduction temperature, the peaks corresponding to the Ni_2P phase at 40.8°, 44.7°, 47.3°, 54.2°, 55.0°, and 74.8° (PDF: 65-1989) become more intense and sharper. There are two possible reasons for this. One reason is that when the reduction temperature increased, more active P species such as PH_3 were formed that promoted formation of the Ni_2P phase. The second reason is that Ni_2P would aggregate into larger particles because of the higher reduction temperature used.

For the Ni–P/Ti/Al–I-1.0-673 K sample, the $Ni_{12}P_5$ phase was detected at 38.4°, 41.7°, 44.4°, 46.9°, and 48.9° (PDF: 65-1623). Ni_2P was not obtained for the sample prepared with an initial P/Ni mole ratio of 1.0, probably because of insufficient P and partial loss of P because of formation of PH_3 or P during the reduction process. With an increase in P/Ni ratio, the pure Ni_2P phase was detected and the Ni_2P peaks became sharper; a possible reason is that with the increase in P/Ni ratio, more Ni_2P active phase was formed.

For the samples prepared by method II, no peaks corresponding to Ni_2P were observed for Ni–P/Ti/Al–II-1.5, which may be attributed to the relatively low P/Ni ratio used. Although the optimal $H_2PO_2^-/Ni^{2+}$ mole ratio was determined to be 1.5 in our previous work,[14] the effect of P/Ni mole ratios on the TiO_2–Al_2O_3 supported catalysts has not been studied. As method II has the advantage of low reaction temperature needed for the preparation of the Ni_2P phase, it is worthwhile further investigating the effect of P/Ni ratios on the physicochemical properties and catalytic performance of Ni–P/TiO_2–Al_2O_3 catalysts. As shown in Fig. S1,† with an increase in the initial P/Ni mole ratio,

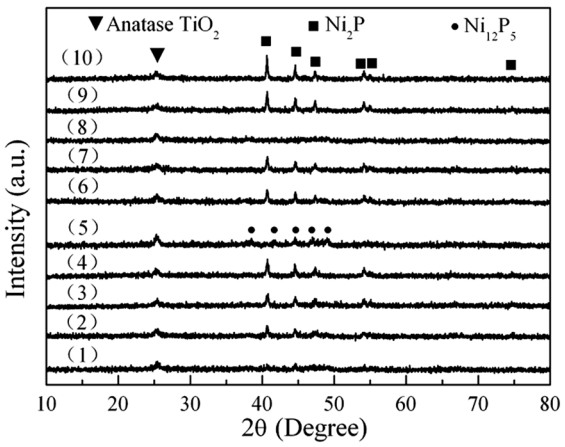

Fig. 1 XRD patterns of Ni–P/TiO_2–Al_2O_3 catalysts prepared by different methods: (1) Ni–P/Ti/Al–I-1.5-573 K (2) Ni–P/Ti/Al–I-1.5-673 K, (3) Ni–P/Ti/Al–I-1.5-773 K, (4) Ni–P/Ti/Al–I-1.5-873 K, (5) Ni–P/Ti/Al–I-1.0-673 K, (6) Ni–P/Ti/Al–I-2.0-673 K, (7) Ni–P/Ti/Al–I-2.5-673 K, (8) Ni–P/Ti/Al–II, (9) Ni–P/Ti/Al–III, and (10) Ni–P/Ti/Al–IV.

the peaks corresponding to the Ni_2P phase become more intense and sharper, which may be attributed to more Ni_2P phase being formed. While the intensity of the Ni_2P phase decreased when the P/Ni ratio further increased to 4.0, the possible reason is that the excess P evolved during the reduction deposits on the outer surface of the Ni_2P catalysts.

Fig. 1 also shows the Ni_2P/TiO_2–Al_2O_3 catalysts prepared by methods III and IV; the peaks corresponding to the Ni_2P phase are sharper than for the samples prepared by methods I and II. The reason is that a much higher reduction temperature (923 K) was employed in methods III and IV and the Ni_2P would aggregate into larger particles. Compared with the Ni–P/Ti/Al–III sample , the Ni_2P phase of Ni–P/Ti/Al—IV showed a slightly greater intensity; the likely reason is that the Ni–P/Ti/Al–IV sample underwent a longer treatment time in the high-temperature region.

3.2. Textural characterization

The textural characterization of supports and catalysts is presented in Table 1. The specific surface areas of pseudoboehmite and γ-Al_2O_3 are 185 and 193 $m^2\ g^{-1}$, respectively. For the TiO_2–Al_2O_3 composite, compared with the pure γ-Al_2O_3, the incorporation of Ti causes an obvious decrease in the surface area. As shown in Table 1, compared with the TiO_2–Al_2O_3 support, the surface area and pore volume of all of the Ni–P/TiO_2–Al_2O_3 catalysts decreased rapidly because of the deposition of P and Ni on the support surface. Similar results were reported previously[27,28] of a remarkable decrease in specific surface areas of the supported Ni_2P catalysts compared with the original support.

For the samples prepared by method I, the surface area increased slightly and then decreased with an increase in the reduction temperature. A possible reason is that the catalyst suffers a more serious loss of surface area and pore volume at higher reduction temperatures. With the increase of P/Ni ratio, the surface area and the pore volume decreased rapidly, which may be due to the deposition of more P on the support surface. The surface area of the Ni–P/Ti/Al–II-1.5 catalyst is 31 $m^2\ g^{-1}$, and the surface area and pore volume decreased with increasing P content, which could be due to the deposition of more P on the support surface (Table S1, ESI†). For the Ni_2P/TiO_2–Al_2O_3 catalysts prepared by methods III and IV, these two samples both showed a very low specific surface area; this could be the result of the deposition of P and Ni on the support surface and the crystallite agglomeration at the high reduction temperature.

Table 1 Textural properties of supports and catalysts

Supports and catalysts	S_{BET} ($m^2\ g^{-1}$)	Average pore size (nm)	Pore volume ($cm^3\ g^{-1}$)
Pseudoboehmite	185	3.8	0.23
Al_2O_3	193	4.3	0.35
Ti/Al	157	4.3	0.29
Ni–P/Ti/Al–I-1.5-573 K	11	3.8	0.03
Ni–P/Ti/Al–I-1.5-673 K	12	3.8	0.03
Ni–P/Ti/Al–I-1.5-773 K	9	5.5	0.03
Ni–P/Ti/Al–I-1.5-873 K	6	4.8	0.02
Ni–P/Ti/Al–I-1.0-673 K	49	4.3	0.09
Ni–P/Ti/Al–I-2.0-673 K	7	4.3	0.02
Ni–P/Ti/Al–I-2.5-673 K	3	4.3	0.01
Ni–P/Ti/Al–II	31	3.8	0.05
Ni–P/Ti/Al–III	4	4.3	0.02
Ni–P/Ti/Al–IV	5	4.3	0.02

3.3. TEM analysis

TEM images of various catalysts are shown in Fig. 2. A TEM image of the Ni–P/Ti/Al–I-1.5-673 K catalyst prepared by method I is shown in Fig. 2(a); the nickel phosphide particle sizes ranged from approximately 10 to 90 nm. For the Ni–P/TiO_2–Al_2O_3 catalyst prepared by method II, Fig. 2(b) shows that the nickel phosphide particle sizes ranged from approximately 5 to 20 nm. To determine the species of the Ni–P/Ti/Al–II-1.5 catalyst, the magnified high-resolution TEM images of selected frames are shown in Fig. S2.† One photograph of the sample yields *d*-spacing values of 0.507 nm, consistent with the *d*-spacing value for {1 0 0} crystallographic planes of the Ni_2P phase. Another photograph yields *d*-spacing values of 0.234 nm, consistent with the *d*-spacing value for {1 1 2} crystallographic planes of the $N_{12}P_5$ phase. The results indicate that not only a Ni_2P phase was formed on the TiO_2–Al_2O_3 support, but also a $Ni_{12}P_5$ phase. This should be attributed to the fact that the phosphorus source is not totally reduced in method II. TEM images of the Ni_2P/TiO_2–Al_2O_3 catalyst prepared by method III and method IV are shown in Fig. 2(c) and (d), respectively. Results indicated that most of the Ni_2P particles are larger than 50 nm, which can be attributed to the high reduction temperature used. The TEM results are consistent with the XRD results, *i.e.*, the sample with sharper Ni_2P peaks showed larger Ni_2P crystal sizes.

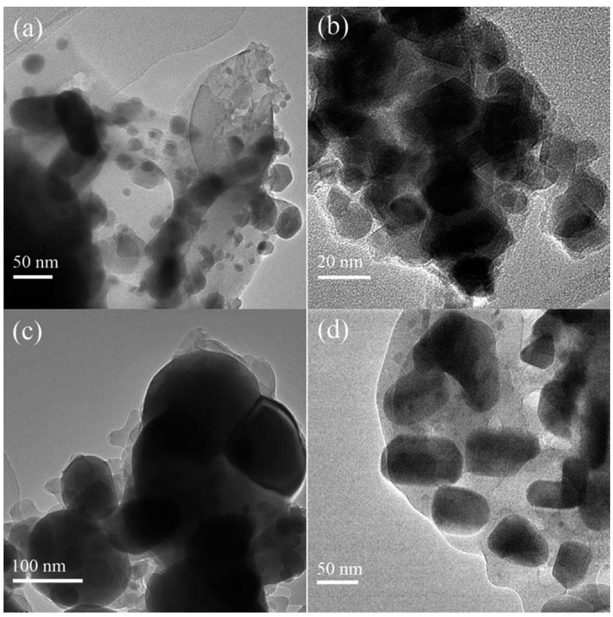

Fig. 2 TEM images of various Ni–P/TiO_2–Al_2O_3 catalysts: (a) Ni–P/Ti/Al–I-1.5-673 K, (b) Ni–P/Ti/Al–II, (c) Ni–P/Ti/Al–III, and (d) Ni–P/Ti/Al–IV.

3.4. Infrared absorption spectroscopy analysis

Fig. 3 shows the IR spectrum of Ni–P/TiO_2–Al_2O_3 catalysts prepared by different methods. In agreement with the previous report,[28] the bands appearing at 1636 and 3450 cm^{-1} can be assigned to the O–H stretching vibration bands, showing the presence of absorbed water and crystalline water in the catalyst. The IR band at 579 cm^{-1} corresponds to the characteristic vibration of Ni–P stretching and the band at 1120 cm^{-1} is ascribed to the existence of $AlPO_4$.

Comparing the IR spectra of catalysts prepared by method I, the peak intensity of $AlPO_4$ becomes stronger when increasing the reduction temperature or increasing the P/Ni ratio, indicating that increasing the reduction temperature and the P/Ni ratio both favor the formation of $AlPO_4$. For the catalyst prepared by method II, it is shown that the peak intensity of $AlPO_4$ is stronger than the Ni–P/Ti/Al–I-1.5-673 K catalyst prepared by method I. From Fig. 3, it can also be seen that the samples prepared by methods III and IV show much stronger peak intensities at 1120 cm^{-1} than the catalysts prepared by method I, which can be attributed to the high reduction temperature (923 K) employed in this procedure. It is obvious that the catalyst Ni–P/Ti/Al–I-1.5-673 K prepared by method I shows much weaker peak intensity at 1120 cm^{-1} than other catalysts, indicating that method I can suppress the formation of $AlPO_4$ more effectively; a possible reason being the relatively low reduction temperature (673 K) and the flowing hydrogen used in this method.

3.5. XPS analysis

The XPS spectra in the Ni(2p) and P(2p) regions for various Ni–P/TiO_2–Al_2O_3 catalysts are shown in Fig. 4. The peaks in the XPS spectrum for the Ni_2P catalyst have been assigned previously.[27–33] As shown in Fig. 4(a), all spectra were decomposed taking into account the spin-orbital splitting of Ni $2p_{3/2}$ and Ni $2p_{1/2}$ lines and the presence of satellite peaks. The Ni $2p_{3/2}$ core level spectrum consists of three contributions, in which the first is assigned to $Ni^{\delta+}$ in the Ni_2P phase and centered at 852.5–853.4 eV, and the second at 854.8–857.6 eV, corresponding to Ni^{2+} ions, possibly interacting with phosphate ions as a consequence of a superficial passivation. The third one is the broad shakeup satellite peak centered at approximately 5 eV higher than that of the Ni^{2+} species. As shown in Fig. 4(a), the catalysts all show an obvious peak centered at 853.1 eV, indicating the formation of Ni_2P in the catalyst. Other broad peaks, centered at the high binding energy side, are assigned to the Ni $2p_{1/2}$ signals.[27–33]

With regards to the P $2p_{3/2}$ binding energy, the spectra corresponding to various Ni–P/TiO_2–Al_2O_3 catalysts (Fig. 4(b)) at 134.3 eV is assigned to P^{5+} species because of the superficial oxidation of Ni_2P particles and the peak at 129.9 eV is attributed to P on the Ni_2P phase.[27–33] Similar to the previous reports,[27–33] all of the samples show broad bands at 133–135 eV, which are assigned to P^{5+} (phosphate) species, indicating that there is a large amount of phosphate over the catalysts. As shown in Fig. 4(b), the Ni_2P phase in the sample of Ni–P/Ti/Al–II is so small that the $P^{\delta-}$ is hardly observed, while other catalysts show an obvious peak at 129.9 eV, which is consistent with the XRD results. The superficial P/Ni atomic ratios of various catalysts were obtained by the XPS analysis (Table 2), compared with the theoretical ratio corresponding to precursors, it can be seen that there is an enrichment of phosphorous on the surface of catalysts.

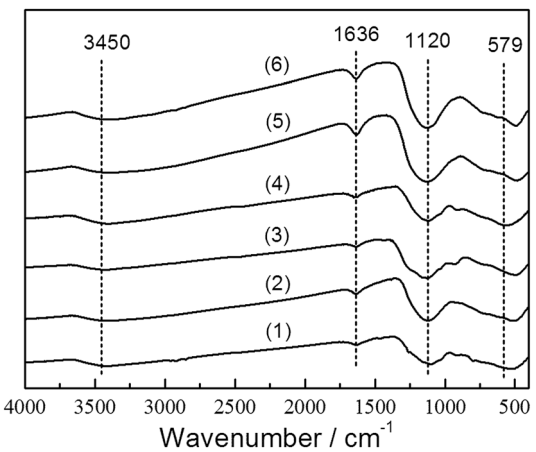

Fig. 3 IR spectra of Ni–P/TiO_2–Al_2O_3 catalysts prepared by different methods: (1) Ni–P/Ti/Al–I-1.5-673 K, (2) Ni–P/Ti/Al–I-1.5-873 K, (3) Ni–P/Ti/Al–I-2.5-673 K, (4) Ni–P/Ti/Al–II, (5) Ni–P/Ti/Al–III, and (6) Ni–P/Ti/Al–IV.

3.6. CO uptake

CO chemisorption capacities for various Ni–P/TiO_2–Al_2O_3 catalysts, which indicate the number of active nickel sites (n_{CO}), are compiled in Table 2. Compared with those reported in the literature,[11,12,17,34,35] the Ni–P/TiO_2–Al_2O_3 catalysts show much lower values of CO uptake. The main reason can be attributed to the much lower surface area and the relatively larger particle sizes of Ni_2P phase of the catalysts, which led to the decrease in the amount of exposed nickel atoms used for adsorption of CO. The low CO uptake over Ni–P/TiO_2–Al_2O_3 catalysts prepared using method III and method IV is easily accountable, which can be attributed to the large size of the Ni_2P particles (>50 nm) because of the high reduction temperature used. Although the Ni–P/Ti/Al–II catalyst possesses the smallest particle size, it also showed a very low CO uptake value, which may be due to the higher surface P/Ni atom ratio than other methods and the low amount of Ni_2P formed. Although CO molecules may adsorb on P sites, their amount may be very small.[36] Similar results were also obtained in the previous report, which is that the excess P covers on the outer surface of the catalyst would lead to the decrease in the amount of exposed nickel atoms used for adsorption of CO.[17] Compared with Ni–P/TiO_2–Al_2O_3 catalysts prepared using other methods, the highest values of CO uptake of the Ni–P/Ti/Al–I-1.5-673 K catalyst would be expected to be due to the relatively high density and the moderate particle sizes of Ni_2P phase.

4. HDS performance

As the main aim of this research was to develop a more feasible way to prepare the highly active Ni_2P/TiO_2–Al_2O_3 catalyst, for

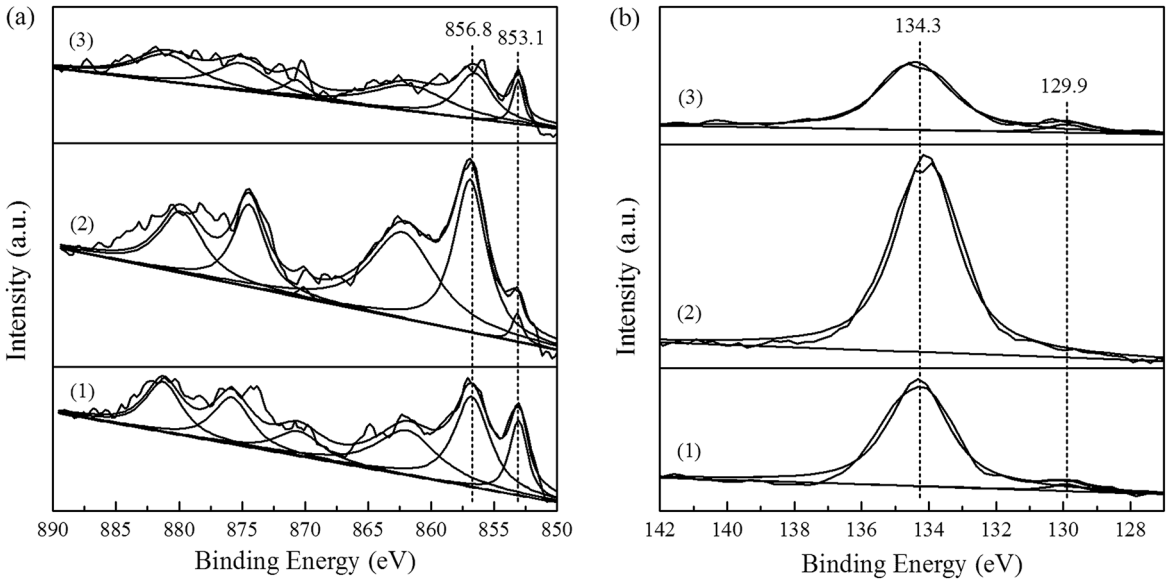

Fig. 4 XPS spectra of Ni–P/TiO_2–Al_2O_3 catalysts prepared by different methods: (1) Ni–P/Ti/Al–I-1.5-673 K, (2) Ni–P/Ti/Al–II, and (3) Ni–P/Ti/Al–III.

comparison, the catalytic performance of Ni–P/TiO_2–Al_2O_3 catalysts prepared by different methods were tested under the same HDS conditions. The DBT conversion and CO uptake were used to calculate the HDS TOF for the catalysts.[17,29] The TOF was calculated using eqn (1). All of the catalytic activities were tested using the eighth-hour liquid products after a stabilization period.

The effect of the reduction temperature on the catalytic performance of Ni–P/TiO_2–Al_2O_3 catalysts prepared by method I is shown in Fig. 5(a). Fig. 5(a) shows that with the increase in the reduction temperature, the DBT conversion initially increased and then decreased when the reduction temperature increased to 873 K. This can be attributed to more Ni_2P active phase being formed when the reduction temperature initially increased, as proved by the XRD results, while more $AlPO_4$ was formed when the reduction temperature further increased to 873 K, as proved by the IR results. Larger Ni_2P particles would also be formed at a higher reduction temperature. The effect of the P/Ni ratio on the catalytic performance of Ni–P/TiO_2–Al_2O_3 catalysts prepared by method I was also tested using the eight-hour liquid products. Fig. 5(b) shows that with an increase in the P/Ni mole ratio, the DBT conversion initially increased from 88.4% (P/Ni = 1.0) to 100.0% (P/Ni = 1.5) and then decreased sharply to 10.5% (P/Ni = 2.5). The likely reason is that, with the increase in P/Ni mole ratio, more Ni_2P active phase was initially formed, as proved by the XRD results, while excess P was formed on the catalyst surface when the P/Ni ratio further increased, which resulted in the Ni_2P active phase being blocked, and thus the catalyst shows low HDS activity. Brunauer–Emmett–Teller (BET) analysis also showed that, compared with the initial P/Ni mole ratio of 1.5, the surface area of Ni–P/TiO_2–Al_2O_3 catalysts decreased noticeably with increasing P/Ni mole ratio.

As shown in Scheme 1, the HDS of DBT involves two parallel pathways: direct desulfurization (DDS) and hydrogenation (HYD). DDS leads to the formation of biphenyl (BP), while HYD yields mainly cyclohexylbenzene (CHB). Because the transformation of BP to CHB is negligible in the presence of DBT, BP selectivity is used as a measure of DDS pathway, and CHB represents the HYD pathway.[37] The product distribution obtained with various catalysts prepared by method I is shown in Fig. 5; two main products were detected: biphenyl (BP) and cyclohexylbenzene (CHB). The results showed that BP is formed in greater proportion in all cases, with direct desulfurization (DDS) being the favored reaction route, which is the same as reported in the literature.[27,28]

Table 2 Superficial P/Ni ratio, CO uptake and DBT HDS performance over Ni_2P/TiO_2–Al_2O_3 catalysts prepared by different methods

Catalysts	Superficial atomic ratio P/Ni	DBT conversion (%)	Selectivity (%)		CO uptake (μmol g^{-1})	TOF (s^{-1})
			BP	CHB		
Ni–P/Ti/Al–I-1.5-673 K	2.41	100	64.7	35.3	4	>0.0060
Ni–P/Ti/Al–II	2.96	72.8	75.9	24.1	2	0.0087
Ni–P/Ti/Al–III	2.60	87.6	62.3	37.7	2	0.010
Ni–P/Ti/Al–IV	—	84.1	63.4	36.6	2	0.010

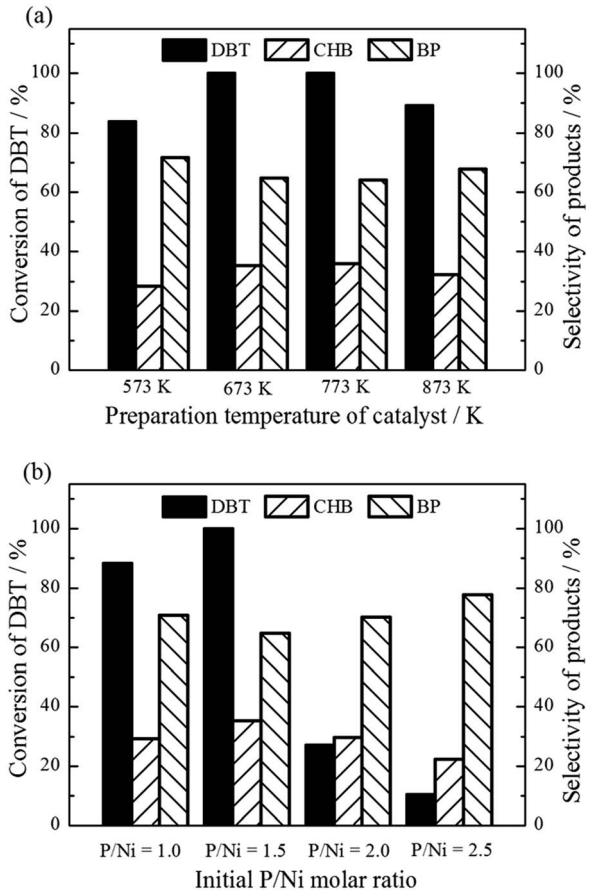

Fig. 5 (a) HDS performance of Ni–P/TiO_2–Al_2O_3 catalysts prepared with different reduction temperatures by method I (P/Ni = 1.5); (b) effect of P/Ni mole ratio on the HDS performance of Ni–P/TiO_2–Al_2O_3 catalysts prepared under a reduction temperature of 673 K by method I. Reaction conditions: 583 K, 3.0 MPa, WHSV = 6 h^{-1}, H_2/oil = 600/1 (v/v).

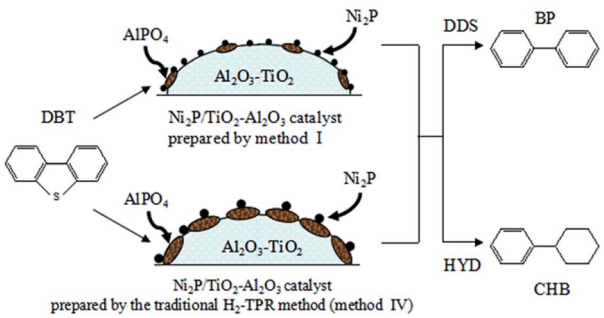

Scheme 1 Reaction pathway of the HDS of DBT over Ni_2P/TiO_2–Al_2O_3 catalysts prepared by methods I and IV.

Table 2 shows that the conversion of dibenzothiophene reached 72.8% for the catalyst of Ni–P/Ti/Al–II. As shown in Fig. S3,† the conversion values decreased with increasing P/Ni mole ratio for the Ni–P/TiO_2–Al_2O_3 catalysts prepared by method II. The likely reason is that, with the increase of P/Ni molar ratio, excess P was formed on the catalyst surface, which resulted in the blocking of the Ni_2P active phase, and thus the catalyst shows low desulfurization activity. As shown in Table S1,† the superficial P/Ni atom ratio of the Ni–P/Ti/Al–II-3.0 catalyst (3.18) shows a higher value than the Ni–P/Ti/Al–II-1.5 catalyst (2.96), which proved the above speculation. BET results (Table S1, ESI†) also showed that, compared with the initial P/Ni molar ratio of 1.5, the surface area of Ni–P/TiO_2–Al_2O_3 catalysts prepared by method II decreased distinctly with increasing P/Ni mole ratio. With regard to the selectivity of different reaction products, the results are much the same as the above analysis, two main products are detected: BP and CHB. BP is formed in greater proportions in all cases, with direct desulfurization (DDS) being the favored reaction route. Table 2 shows the catalytic performance of Ni_2P/TiO_2–Al_2O_3 catalysts prepared by different methods. The results indicate that for the Ni_2P/TiO_2–Al_2O_3 catalysts, the DBT conversion using the DR method is slightly higher than by the H_2-TPR method. Similar to the previous results, two main products are detected, BP and CHB (Table 2). The results show that BP is also formed in greater proportion for the catalysts tested, with DDS being the favored reaction route.

5. Discussion

The results in this paper indicate that Ni_2P/TiO_2–Al_2O_3 catalysts can be synthesized using various methods, while the HDS performance varied a lot. As far as we know, the Ni_2P/TiO_2–Al_2O_3 catalysts reported so far all use the H_2-TPR method and the reduction temperature can be as high as 973 K. The effect of preparation conditions on the Ni_2P/TiO_2–Al_2O_3 catalyst using phosphate-containing precursors has already been studied in previous reports. As the phosphate-containing precursor was used in the preparation of the Ni_2P/TiO_2–Al_2O_3 catalyst in method IV, a high reduction temperature is required because of the strong P–O bond.[26–30] Although the Ni–P/Ti/Al–IV catalyst showed a relatively high value of DBT conversion (84.1%), it is not a good way to prepare the Ni_2P/TiO_2–Al_2O_3 catalyst because of the high temperature required and the TPR steps. As shown in Table 2, the DBT conversion of the Ni_2P/TiO_2–Al_2O_3 catalyst prepared by method III is slightly higher than the catalyst prepared by the H_2-TPR method. Compared with the H_2-TPR method, method III has the advantage of simplicity and low hydrogen consumption, while it is still not a good choice for the preparation of the Ni_2P/TiO_2–Al_2O_3 catalyst, which is due to the high reduction temperature required. In addition, the high reduction temperature also leads to the formation of large phosphide particles and low catalytic activity.

The major advantage of method II is a low preparation temperature (573 K) was required because of employing hypophosphite as the phosphorus source. For the Ni–P/Ti/Al–II-1.5 catalyst, smaller nickel phosphide particles were obtained compared with other methods, but the Ni–P/Ti/Al–II catalyst showed the lowest activity. This should be attributed to the fact that the phosphorus source is not totally reduced in method II, and this not only led to less Ni_2P phase obtained, but also $Ni_{12}P_5$ phase formed. According to previous reports,[25,38] the $Ni_{12}P_5$ has a lower activity than the Ni_2P catalyst. This should be the main

reason that the Ni–P/Ti/Al–II catalyst gave the lowest HDS conversion among different methods. At the same time, the Ni–P/Ti/Al–II catalyst also showed higher superficial P/Ni atomic ratio than other catalysts, which is not beneficial for the reaction between the reactant of DBT and the active phase of nickel phosphide. Although more Ni_2P phase was formed by increasing the P/Ni ratios, the catalytic activity decreased. The reason can be attributed to the fact that the excess P evolved during the reduction deposites on the outer surface of the catalysts, which not only leads to the coverage of the Ni_2P phase, but also leads to the decrease of the surface area and pore volume of the catalysts (Table S1, ESI†).

Ni_2P/TiO_2–Al_2O_3 catalysts prepared by method I showed excellent HDS activity. The main reason can be attributed to the relatively low synthesis temperature and the flowing hydrogen used in method I. For the Ni–P/Ti/Al–I-1.5-673 K catalyst, the formation of $AlPO_4$ was more effectively suppressed, as proved by the IR results, and the formation of active sites, *i.e.*, Ni_2P, was favored. Scheme 1 depicts the schematic views of the difference between Ni_2P/TiO_2–Al_2O_3 catalysts prepared by method I and method IV. The proposed representations are deduced from the above characterizations. The XRD patterns of Ni–P/Ti/Al–I-1.5-673 K catalyst and Ni–P/Ti/Al–IV catalyst are compared separately in Fig. S4,† the results also indicated that the small $AlPO_4$ diffraction peaks can be found at 19.6° and 21.4° for the Ni–P/Ti/Al–IV catalyst, while no typical peaks for $AlPO_4$ are detected clearly for the Ni–P/Ti/Al–I-1.5-673 K catalyst. The results are in accordance with the IR results, which further proved the proposed representations in Scheme 1. Compared with method IV, a less oxidic precursor of P employed in method I enables the Ni_2P phase to be formed at a lower temperature below 673 K, which gives rise to the successful formation of more dispersed Ni_2P phase on the TiO_2–Al_2O_3 support with less $AlPO_4$ phase. As shown in Scheme 1, the conventional temperature-programmed reduction method with use of the nickel phosphate precursor leads to the formation of more $AlPO_4$ phase on the TiO_2–Al_2O_3 support because of the strong interaction between phosphorus and γ-Al_2O_3, which results in a lack of Ni_2P phase. At the same time, the Ni_2P would aggregate to larger particles after reduction at 923 K, which can cause serious damage to the activity of the Ni_2P/TiO_2–Al_2O_3 catalyst.

The relatively low synthesis temperature can weaken the strong interaction between Al_2O_3 and P, but this is not enough, as some by-products were formed in the synthesis of the active phase of Ni_2P, such as HPO_3H^- and H_2O,[16,17] that are harmful to the synthesis of the highly active phase of Ni_2P. The flowing hydrogen not only takes the by-products away, but also promotes the reduction of the Ni and P species, the total effect leading to the formation of the highly active Ni_2P phase. To prove further the effect of flowing H_2, two other catalysts were prepared and their HDS performances were also tested. For these two catalysts, the same reduction temperature and P/Ni ratio were employed as for the Ni–P/Ti/Al–I-1.5-673 K catalyst, one being prepared in static H_2 (denoted as Ni–P/Ti/Al–I-1.5-673-SH) and the other in flowing Ar (denoted as Ni–P/Ti/Al–I-1.5-673-FA). As shown in Fig. S5,† both catalysts show peaks corresponding to $Ni_{12}P_5$, while a very weak Ni_2P peak is also observed for the sample of Ni–P/Ti/Al–I-1.5-673-FA. It can be seen clearly that flowing H_2 is crucial for the formation of Ni_2P through comparative analysis. The HDS results (Fig. S6, ESI†) indicated that the DBT conversion of Ni–P/Ti/Al–I-1.5-673-SH and Ni–P/Ti/Al–I-1.5-673-FA was 72.5% and 86.8%, respectively. Because the DBT conversion reached 100.0% for the Ni–P/Ti/Al–I-1.5-673 K catalyst, it is clear that flowing H_2 is indispensable for the formation of a highly active Ni_2P catalyst. In general, the flowing H_2 under a moderate reduction temperature can cause further reduction of phosphite ions and the formation of $AlPO_4$ was more effectively suppressed in method I, and then the highly active Ni_2P phase was obtained.

In addition, the effects of Ni_2P loadings and the incorporation of TiO_2 on the textural properties and the HDS activities of supported nickel phosphide catalysts were studied by method II as a representative. As shown in Table S2,† the surface area of the Ni_2P/TiO_2–Al_2O_3 catalyst decreased with increasing Ni_2P loadings. Compared with γ-Al_2O_3 supported Ni–P catalysts, the Ni_2P/TiO_2–Al_2O_3 catalyst also showed lower surface area. The HDS results (Fig. S7, ESI†) indicated that the DBT conversion increased with increasing the Ni_2P loadings, which may be attributed to the fact that a more active phase of nickel phosphide was formed. It also can be seen that the Ni_2P/TiO_2–Al_2O_3 catalyst showed a higher DBT conversion (72.8%) than the Ni–P/Al_2O_3 catalyst (62.2%). The reason can be attributed to the fact that the TiO_2–Al_2O_3 composite support can effectively prevent the formation of aluminum phosphates due to the strong interaction between phosphorus and γ-Al_2O_3, which improve the desulphurization activity of the nickel phosphide catalyst. Based on the results obtained above, we can make a conclusion that although increasing the Ni_2P loading and using TiO_2–Al_2O_3 as the support, both have a negative effect on the surface area of the nickel phosphide catalysts, the highest DBT activity was obtained for the TiO_2–Al_2O_3 supported nickel phosphide catalysts with a Ni_2P loading of 30 wt%. In general, the results obtained in the present paper are in accordance with previous reports,[26–28] which are that the introduction of TiO_2 into the γ-Al_2O_3 support can improve the desulphurization activity of Ni_2P catalyst.

6. Conclusions

In the present work, a series of Ni_2P/TiO_2–Al_2O_3 catalysts was successfully prepared using four different methods and the effect of preparation method on the catalytic activity for the HDS of DBT was investigated. For the Ni_2P/TiO_2–Al_2O_3 catalysts prepared using H_2 reduction of a mixture of a $NiCl_2 \cdot 6H_2O$ and $NH_4H_2PO_2$ precursor using a TiO_2–Al_2O_3 composite material as the support (method I), the effect of the P/Ni ratio and reduction temperature on the HDS activity was studied. The results indicated that the Ni_2P/TiO_2–Al_2O_3 catalyst could be synthesized at a low reduction temperature of 573 K, and the catalyst prepared with an initial P/Ni mole ratio of 1.5 and a relatively low reduction temperature of 673 K showed excellent catalytic performance and the conversion of DBT reached 100.0%. For the Ni_2P/TiO_2–Al_2O_3 catalysts prepared by the thermal decomposition of a solid mixture of $NiCl_2 \cdot 6H_2O$ and $NaH_2PO_2 \cdot H_2O$

(method II), the DBT conversion showed a relatively low value of 72.8%. For the Ni_2P/TiO_2–Al_2O_3 catalysts prepared using $NH_4H_2PO_4$ as the phosphorus source, the DR method (method III) showed a slightly higher DBT conversion than the H_2-TPR method (method IV). The IR results indicated that method I can effectively suppress the formation of $AlPO_4$ and favor the formation of Ni_2P, which can be attributed to the relatively low reduction temperature and the flowing hydrogen used in this method. In general, the results obtained in this paper suggest that method I provides an excellent choice for the preparation of the highly active Ni_2P/TiO_2–Al_2O_3 catalyst for the HDS of DBT at a much lower temperature (573 K) than previously reported methods (973 K).

Acknowledgements

This work was financially supported by the NSFC (21376123, U1403293), MOE (IRT-13R30), MOE (113016A), and the Research Fund for 111 Project (B12015).

Notes and references

1 A. Shah, R. Fishwick, J. Wood, G. Leeke, S. Rigby and M. Greaves, *Energy Environ. Sci.*, 2010, **3**, 700–714.
2 V. C. Srivastava, *RSC Adv.*, 2012, **2**, 759–783.
3 X. Q. Wang, P. Clark and S. T. Oyama, *J. Catal.*, 2002, **208**, 321–331.
4 S. T. Oyama, T. Gott, H. Y. Zhao and Y. K. Lee, *Catal. Today*, 2009, **143**, 94–107.
5 R. Prins and M. E. Bussell, *Catal. Lett.*, 2012, **142**, 1413–1436.
6 K. S. Cho, H. R. Seo and Y. K. Lee, *Catal. Commun.*, 2011, **12**, 470–474.
7 S. T. Oyama and Y. K. Lee, *J. Catal.*, 2008, **258**, 393–400.
8 Y. Y. Shu and S. T. Oyama, *Carbon*, 2005, **43**, 1517–1532.
9 Y. Zeng, B. H. Zhao, L. F. Zhu, D. M. Tong and C. W. Hu, *RSC Adv.*, 2013, **3**, 10806–10816.
10 S. F. Yang, C. H. Liang and R. Prins, *J. Catal.*, 2006, **237**, 118–130.
11 J. E. Wang, H. Chen, Y. C. Fu and J. Y. Shen, *Appl. Catal., B*, 2014, **160–161**, 344–355.
12 H. Song, M. Dai, H. L. Song, X. Wan, X. W. Xu and Z. S. Jin, *J. Mol. Catal. A: Chem.*, 2014, **385**, 149–159.
13 Z. Q. Wang, L. X. Zhou, M. H. Zhang, M. Su, W. Li and K. Y. Tao, *Chem.–Asian J.*, 2009, **4**, 1794–1797.
14 Q. X. Guan, W. Li, M. H. Zhang and K. Y. Tao, *J. Catal.*, 2009, **263**, 1–3.
15 Q. X. Guan and W. Li, *J. Catal.*, 2010, **271**, 413–415.
16 G. J. Shi and J. Y. Shen, *J. Mater. Chem.*, 2009, **19**, 2295–2297.
17 H. Song, M. Dai, H. L. Song, X. Wan and X. W. Xu, *Appl. Catal., A*, 2013, **462–463**, 247–255.
18 J. A. Cecilia, A. Infantes-Molina, E. Rodríguez-Castellón and A. Jiménez-López, *J. Catal.*, 2009, **263**, 4–15.
19 A. Infantes-Molina, J. A. Cecilia, B. Pawelec, J. L. G. Fierro, E. Rodríguez-Castellón and A. Jiménez-López, *Appl. Catal., A*, 2010, **390**, 253–263.
20 J. A. Cecilia, A. Infantes-Molina, E. Rodríguez-Castellón and A. Jiménez-López, *J. Phys. Chem. C*, 2009, **113**, 17032–17044.
21 A. J. Wang, M. L. Qin, J. Guan, L. Wang, H. C. Guo, X. Li, Y. Wang, R. Prins and Y. K. Hu, *Angew. Chem., Int. Ed.*, 2008, **47**, 6052–6054.
22 M. F. Li, H. F. Li, F. Jiang, Y. Chu and H. Nie, *Fuel*, 2009, **88**, 1281–1285.
23 S. Sigurdson, V. Sundaramurthy, A. K. Dalai and J. Adjaye, *J. Mol. Catal. A: Chem.*, 2008, **291**, 30–37.
24 J. N. Díaz de León, M. Picquart, L. Massin, M. Vrinat and J. A. de los Reyes, *J. Mol. Catal. A: Chem.*, 2012, **363–364**, 311–321.
25 S. J. Sawhill, K. A. Layman, D. R. Van Wyk, M. H. Engelhard, C. M. Wang and M. E. Bussell, *J. Catal.*, 2005, **231**, 300–313.
26 K. L. Wang, B. L. Yang, Y. Liu and C. H. Yi, *Energy Fuels*, 2009, **23**, 4209–4214.
27 H. Song, M. Dai, Y. T. Guo and Y. J. Zhang, *Fuel Process. Technol.*, 2012, **96**, 228–236.
28 T. Chen, B. L. Yang, S. S. Li, K. L. Wang, X. D. Jiang, Y. Zhang and G. W. He, *Ind. Eng. Chem. Res.*, 2011, **50**, 11043–11048.
29 Q. X. Guan, X. Cheng, R. G. Li and W. Li, *J. Catal.*, 2013, **299**, 1–9.
30 S. J. Sawhill, D. C. Phillips and M. E. Bussell, *J. Catal.*, 2003, **215**, 208–219.
31 H. Song, X. W. Xu, H. L. Song, N. Jiang and F. Y. Zhang, *Catal. Commun.*, 2015, **63**, 52–55.
32 T. Tian, L. H. Ai and J. Jiang, *RSC Adv.*, 2015, **5**, 10290–10295.
33 Y. Pan, Y. Q. Liu and C. G. Liu, *RSC Adv.*, 2015, **5**, 11952–11959.
34 S. T. Oyama, X. Wang, Y. K. Lee, K. Bando and F. G. Requejo, *J. Catal.*, 2002, **210**, 207–217.
35 Y. Y. Shu, Y. K. Lee and S. T. Oyama, *J. Catal.*, 2005, **236**, 112–121.
36 K. A. Layman and M. E. Bussell, *J. Phys. Chem. B*, 2004, **108**, 10930–10941.
37 X. Li, Z. C. Sun, A. J. Wang, X. N. Yang and Y. Wang, *Appl. Catal., A*, 2012, **417–418**, 19–25.
38 T. I. Korányi, A. E. Coumans, E. J. M. Hensen, R. Ryoo, H. S. Kim, É. Pfeifer and Z. Kasztovszky, *Appl. Catal., A*, 2009, **365**, 48–54.

